

High Vibration Damping in In Situ In-Zn Composites

Samuel P. Balch^{*} and Roderic S. Lakes

*Department of Engineering Physics, University of Wisconsin-Madison
Madison, WI 53706, USA*

**sbalch@wisc.edu*

Indium zinc in situ composites were fabricated and their viscoelastic properties studied over 8.5 decades of frequency. Material with 5% indium by weight was found to have a stiffness damping product (the figure of merit for damping layers) of 1.9 GPa at 10 Hz; 3 times better than the peak of polymer damping layers and over a wider frequency range. Material with 15% indium had a stiffness damping product of 1.8 GPa. The indium segregated in a platelet morphology, particularly favorable for attaining high damping from a small concentration, as predicted by viscoelastic composite theory.

Keywords: internal friction; heterostructures; dynamic mechanical analysis, damping layer, noise control

Preprint adapted from [Balch, S. and Lakes, R. S., High vibration damping in in situ In-Zn composites, Functional Materials Letters, 8, \(5\) 1550059 \(4 pages\) \(2015\).](#)

1. Introduction

Materials that are stiff and have high internal friction are of practical interest to reduce vibrations and noise in structures and machinery. Structural metals typically have low damping, a $\tan \delta$ of 10^{-5} to 10^{-3} . To reduce vibrations and noise in machinery, viscoelastic layers are attached to structural plates. For axial or bending vibration of a bar or plate with a damping layer, the effective loss depends on the layer's Young's modulus E and damping: $\tan \delta_{eff} \propto E_{layer} \tan \delta_{layer}$. Most common materials have either high stiffness and low internal friction or low stiffness and high internal friction. Polymer damping layers designed for maximum performance are in the transition region between glassy and rubbery behavior; they have a maximum figure of merit $E \tan \delta$ of 0.6 GPa^{1,2}. The peak in damping is strongly dependent on frequency and on temperature, a drawback for many applications.

High damping metals³ are available; they are stiff and provide structural rigidity in contrast to polymers. For example zinc-aluminum alloys⁴ have been studied but they provide $\tan \delta$ only about

0.001 above 1 kHz. β -TI alloys with high oxygen solid solution have provided high damping, but only at elevated temperatures⁵. Cu-Mn alloys have been used in naval ship propellers⁶ to reduce vibration and noise emission; they are nonlinear and only provide high damping with high displacement. Shape memory metals⁷ can exhibit high damping over a range of temperature but they are nonlinear. Many such available metals are nonlinear and only offer enhanced damping for large amplitude vibration. It is possible to obtain better performance with designed composite materials^{8,9}; even so, the simplicity of macroscopically homogeneous material can be appealing.

In the present study, indium zinc alloys were prepared and the viscoelastic properties determined over 8.5 decades of frequency.

2. Experimental Procedures

The specimens were prepared by melting and mixing measured quantities of granular indium and zinc obtained from Alfa Aesar. The molten metal was poured into cylindrical molds and cooled.

^{*}Corresponding author.

Viscoelastic properties were measured using broadband viscoelastic spectroscopy in torsion, resonant ultrasonic spectroscopy and wave ultrasound at ambient temperature 22°C. The structure of the material was studied using optical microscopy and energy dispersive x-ray spectroscopy (EDS) was used to verify the composition of the phases in the micrographs, as follows.

Broadband viscoelastic spectroscopy (BVS) ¹⁰ was used to determine the viscoelastic properties of the materials. It is capable of measuring across 11 decades of frequency, from creep testing to ultrasonic testing without appeal to time/temperature superposition. In BVS, the specimen is mounted to a support rod with fixed-free end conditions. Torque was applied through the interaction of a Helmholtz coil and a high intensity neodymium permanent magnet bonded to the free end of the specimen. The angular deflection of the specimen was measured by reflecting a laser beam off a mirror bonded to the specimen into a beam position detector, quad cell, type New Focus model 2901. Torque was inferred from the current through the coil, evaluated from the voltage across a resistor in series with the coil. Calibration was done using a specimen of a well known aluminum alloy. Torsion or bending studies can be performed via orthogonal coils; torsion was used in the present study because a wider frequency range is possible.

The shear modulus was inferred from the ratio of torque required to angular deflection. Shear modulus taken as the absolute value $|G^*|$ was then converted to Young's modulus E using the Poisson's ratio of zinc. Internal friction, or damping, is characterized by the tangent of the material phase angle δ between sinusoidal waveforms in stress and strain. Material phase is equivalent to structural phase between torque and angle, well below resonance; at higher frequencies a correction for resonance is applied.

In the sub-resonant regime, data for magnitude and phase were collected with a lock-in amplifier (Stanford Research Systems, SR 850) or from Lissajous figures on a digital oscilloscope. In the Lissajous figure method, the angle and torque signal are displayed on an oscilloscope as an $x - y$ plot. Linear behavior entails an elliptic plot; the ellipse becomes a straight line if the material is elastic with no damping. The structural phase angle is found from the width of the elliptic figure near the origin to total width of the figure ². Stiffness is determined from the ratio of torque to angle signals of the figure. The Lissajous figure method was used to corroborate the lock-in results.

In the resonant regime, the internal friction of the specimen was found by measuring the qual-

ity factor of the resonant peaks. Specifically, $\tan \delta \approx \frac{1}{\sqrt{3}} \frac{\Delta f}{f_0}$ in which the full width at half maximum of frequency f is Δf . Use of a small magnet, no wider than the specimen, allows study of higher modes, but amplitude of the signal below resonance is then reduced.

Resonant ultrasonic spectroscopy (RUS) ¹¹ is a method of measuring the moduli and damping of a material by exciting a sample with a transducer and sensing the resonant response with another transducer. The specimen is cut to a shape such as a cube or short cylinder. The fundamental mode reveals the shear modulus G via an analytical solution. The lowest natural frequency f_1^{cyl} for a cylinder of length L is, for free torsional vibration in the absence of end inertia, $f_1^{cyl} = \frac{1}{2L} \sqrt{\frac{G}{\rho}}$ in which ρ is density. The diameter was equal to the length. Damping was determined as in BVS resonance above by measuring the quality factor of the resonant peaks. Short cylinders were cut from the BVS specimens with a wet, low speed, diamond saw that does not change the material properties of the specimen.

Wave ultrasound is a technique in which a piezoelectric transducer passes compression or shear waves through a specimen at an ultrasonic frequency. A second transducer senses the wave. Using this method, wave attenuation was measured. This was done by measuring the magnitude of the sensed wave while maintaining the same coupling force for several specimens of different lengths. The exponential decay of the magnitude of the response is the attenuation. Damping was inferred from attenuation.

Linearity was verified by repeating measurements at different input amplitudes. Strain levels were typically below 10^{-5} , well within the linear range. Also, the shape of Lissajous figures as narrow ellipses reveals linearity of response.

Specimens for microscopic study were cut with a diamond saw and mounted in epoxy resin. The specimens were then ground and polished with graded abrasives. The finest polish was with 50 nm colloidal silica. The specimens were etched with 10 second exposure to 1:10 hydrochloric acid, water etchant. Optical micrographs were captured using an Olympus (Melville, NY) type BH2-1 microscope with a digital camera and image capture system.

As for composition mapping, an un-etched specimen was mounted in a LEO 1530 scanning electron microscope. An image was formed using the back-scattered electron signal. Back-scattered electrons indicate the atomic weight of the material. The two phases in the specimen were clearly visi-

ble. Energy dispersive x-ray spectroscopy was used to determine the atomic composition of the phases.

3. Results

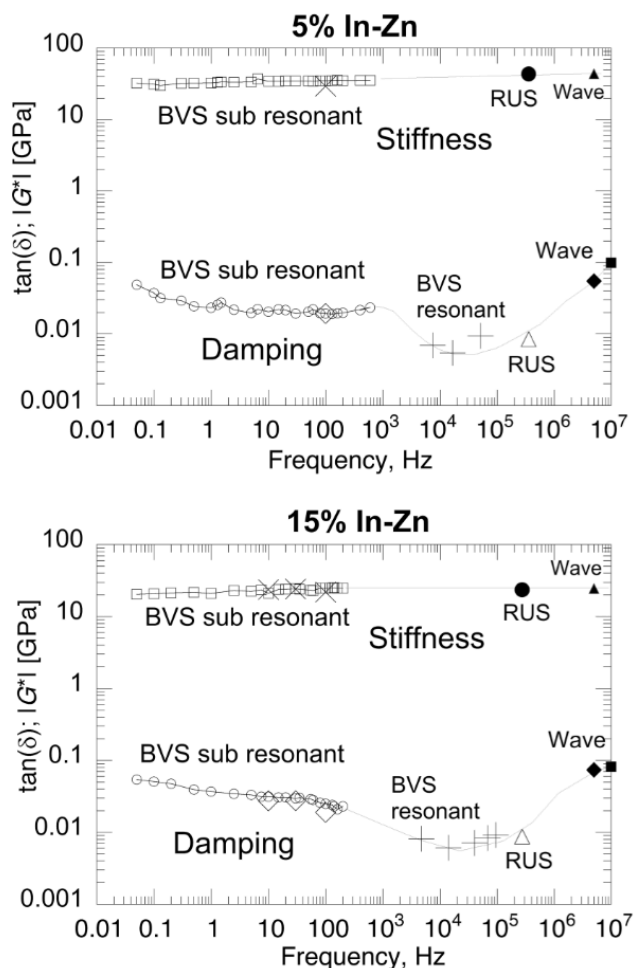


Fig. 1. Experimental results for 5% and 15% indium composites. The \circ and \square markers correspond to BVS lock-in method. The \times and \diamond markers to BVS Lissajous figure method. The \blacksquare marker to ultrasonic longitudinal waves and the \blacklozenge and \blacktriangle correspond to ultrasonic shear waves.

Specimens with 5% and 15% indium by weight were tested. As indium content increased, damping increased and stiffness decreased. Best performance, quantified by the product of the modulus of elasticity and the damping, was given by the 5% indium alloy, which had a stiffness-damping product of 2.0 GPa at 1 Hz and 1.9 GPa at 10 Hz. This is more than 3 times the stiffness-damping product of conventional polymers. The shear modulus and damping of this material is shown in Figure 1 over 8.5 decades of frequency.

Pure cast zinc is itself a high damping material over a wide range of frequency¹² with $\tan \delta$ of about 0.01. Addition of 5% indium reduced the stiffness

by 30% but increased damping by 90%, leading to a 40% increase in the damping layer figure of merit. A composition of 15% indium, 85% zinc also provided high performance. This alloy had a stiffness-damping product of 2.0 GPa at 1 Hz and 1.8 GPa at 10 Hz. The attenuation was 593 nepers per meter for shear waves 5 MHz and was 751 nepers per meter for longitudinal waves at 10 MHz. The $\tan \delta$ implied by this attenuation was computed and the shear modulus and damping of this material over about 8.5 decades of frequency is displayed in Figure 1. The high damping for frequencies above 1 MHz is attributed to scattering of the waves from the heterogeneous microstructure.

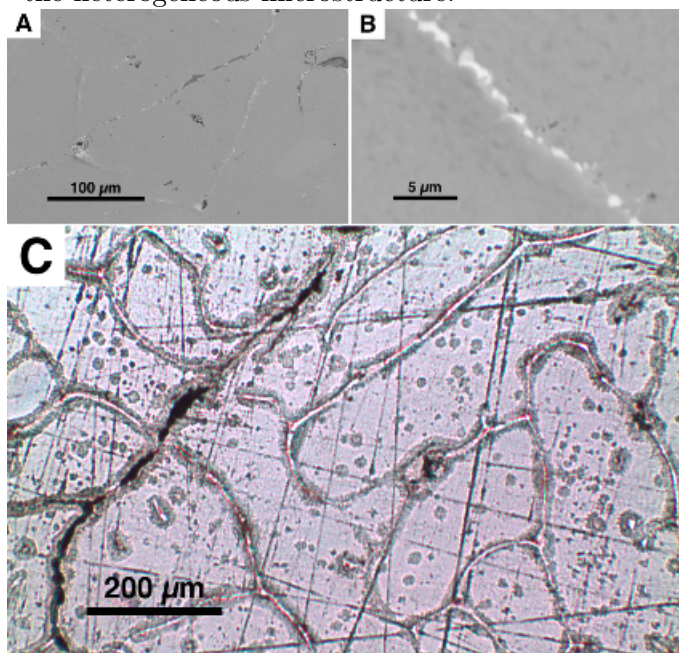


Fig. 2. (A) A grain of zinc with indium in the grain boundaries. (B) Close up of a grain boundary. The lighter phase was confirmed to be indium and the grey phase was confirmed to be zinc using EDS. (C), Optical microscope image of 5% indium sample. Image taken at 10x magnification. Zinc grains are visible, with indium appearing in grain boundaries.

Microscopy revealed the structure of the alloy. A grain of zinc with indium in the grain boundaries is shown in Figure 2A. This image was created using the back-scattered electron signal in a scanning electron microscope. Higher atomic numbered constituents appear lighter. The light grey phase is zinc, atomic number 30, the white phase is indium, atomic number 49. The dark material is the silica polishing media. The elemental composition of the phases was verified by zooming in on a grain boundary, shown in Figure 2B, and using EDS. This confirmed that the grey material is zinc and the white material is indium. The grain structure is more visible in an optical microscope image of an etched

specimen. This is shown in Figure 2C. Zinc grains are visible and indium appears in grain boundaries.

4. Analysis

Analysis is based on extremal behavior of elastic composites. The upper and lower bounds for elastic moduli of isotropic two phase composites after Hashin and Shtrikman¹³ are attainable by hierarchical structures. Composites with sufficiently dilute platelet inclusions¹⁴ approach the upper bound formulae. Viscoelastic properties were analyzed by applying the elastic - viscoelastic correspondence principle to the elastic formulae, and separating real and imaginary parts to obtain a map of stiffness vs. damping. The curves are not bounds but they are close to the viscoelastic bounds. This procedure shows that structures that give rise to minimal stiffness vs. volume fraction in the elastic case also provide maximal values of the product of damping and stiffness in the viscoelastic case¹⁵. Composites with soft, high loss platelets or stiff spheres are therefore favored.

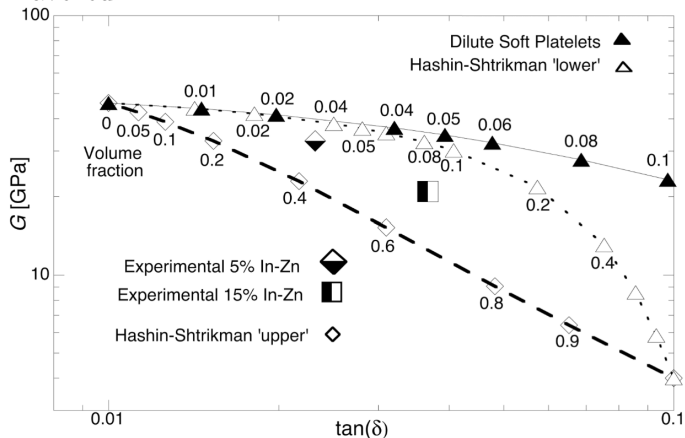


Fig. 3. Comparison with theory and experiment at 1 Hz. Theoretical curves are based on Hashin-Shtrikman formulae and on the analysis of an isotropic composite with dilute platelet inclusions.

The analytical shear modulus and $\tan \delta$ for a composite with a zinc matrix and randomly oriented indium platelets is shown in Figure 3 with the experimental results at 1 Hz. The 5% indium composite approaches the theoretical behavior of a platelet reinforced composite. The 15% indium composite is not as favorable but is still an improvement over pure zinc. Perfect agreement with theory is not to be expected because the damping of metals depends on dislocation density which in turn depends on the history of deformations such as those which occur during casting and phase segregation.

5. Discussion

The indium-zinc exhibited high damping and a high product of stiffness and damping in the linear range of behavior, at small oscillatory strain. This is in contrast to most high damping metals reported heretofore; these require a substantial amplitude of vibration to achieve damping.

Segregation of indium and zinc during solidification occurs as a result of the mutual insolubility of the phases. The zinc phase forms as grains and the indium is sequestered as thin layers in the grain boundaries. This structure constitutes a *in-situ* composite in which the zinc is the matrix and the indium behaves as randomly oriented platelet inclusions. Such a morphology is favorable for obtaining a maximum product of modulus and damping. By contrast, dilute spherical inclusions of a soft, high damping material would not significantly enhance the damping. Indeed, indium-aluminum materials were made in an effort to achieve high damping¹⁶ but without design of inclusion shape. They exhibited elevated damping near the melting point of indium but not at ambient temperature. The round shape of the soft inclusions was not favorable in this case.

The mechanism of the damping in indium is considered to be dislocation drag at high homologous temperature. The melting point of indium is only 156°C. The damping in zinc is also likely to be related to dislocations, but existing models do not account for the relatively flat response vs. frequency¹².

The figure of merit of these alloys can be compared to other materials in Figure 4. Both 5% indium and 15% indium alloys can be found far into the upper right corner, in the best performance region. Some composites (W-InSn)⁸ provide proof of concept of higher performance, particular at lower frequency down to 10^{-3} Hz at the right in the stiffness-loss map. These composites are too dense to be practical. The InSn used in these composites is itself a high damping material for which the highest damping is at the lowest frequency, 10^{-3} Hz at the right in Figure 4; its dependence on frequency f is $\tan \delta \propto f^n$ with $n = -0.2$. The present 5% material is much less dependent on frequency ($n = -0.087$), a benefit for damping in the acoustic range or for a broad band of frequencies. Low density composites based on SiC-InSn⁹ could be made with In-Zn rather than In-Sn as a matrix.

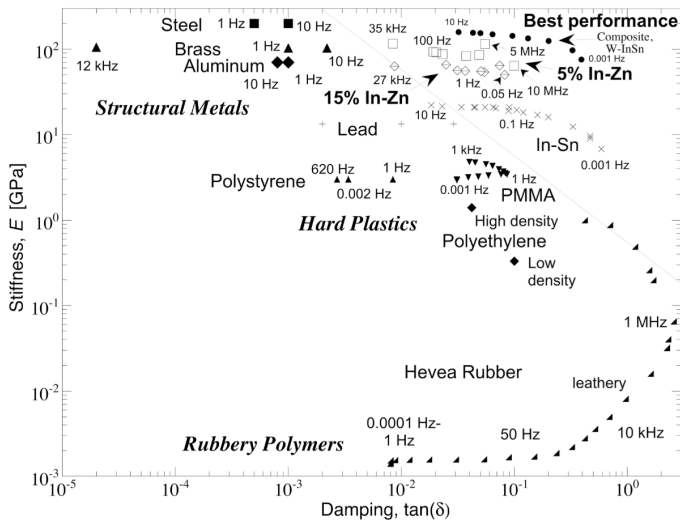


Fig. 4. Stiffness-loss map of conventional materials and designed high performance materials. Best performance, as quantified by stiffness-damping product, is in the top right region.

Acknowledgment

Support from the ARO is gratefully acknowledged.

References

1. R.N. Capps, L. L. Beumel, *Sound and Vibration Damping with Polymers*, Eds. R. D. Corsaro and L. H. Sperling, Chapter 4 (American Chemical Society, Washington DC, USA, 1990), pp. 63-78.

2. R. S. Lakes, *Viscoelastic Materials*, (Cambridge University Press, Cambridge, UK, 2009).
3. I. G. Ritchie, Z. L. Pan, *Met. Trans.*, **22A**, 607 (1991).
4. I. G. Ritchie, Z. L. Pan, F. E. Goodwin, *Met. Trans.*, [22A, 617 (1991).
5. F. Yin, S. Iwasaki, D. Ping, K. Nagai, *Adv. Mater.*, **18**, 1541 (2006).
6. I. G. Ritchie, K. W. Sprungmann, M Sahoo, *J. de Phys.*, **46**, C10-409 (1985).
7. R. R. Hasiguti, K. Iwasaki, *J. Appl. Phys.*, **39**, 2182 (1968).
8. M. Brodt, R. S. Lakes, *J. Composite Mater.*, **29**, 1823 (1995).
9. M. Ludwigson, C. C. Swan, R. S. Lakes, *J. Composite Mater.*, **36**, 2245 (2002).
10. T. Lee, R. S. Lakes, A. Lal, *Rev. of Scientific Instruments*, **71**, 2855 (2000).
11. A. Migliori, J. L. Sarrao, *Resonant Ultrasound Spectroscopy*, (Wiley VCH, Weinheim, Germany, 1997).
12. Y. C. Wang, M Ludwigson, R. S. Lakes, *Mater. Science and Engineering A*, **370**, 41 (2004).
13. Z. Hashin, S. A. Shtrikman, *J. Mech. Phys. Solids*, **26**, 127 (1963).
14. A. N. Norris, *Int. J. Solids, Structures*, **26**, 663 (1990).
15. C. P. Chen, R. S. Lakes, *J. Mater. Science*, **28**, 4299 (1993).
16. A. K. Malhotra, D. C. Van Aken, *Acta Metall. Mater.*, **41** 1337 (1993).